Investigation of Interpolation Strategies for Hybrid Schemes in Computational Aeroacoustics

Andreas Hüppe[1], Manfred Kaltenbacher[1]

[1] *Vienna University of Technology, 1060 Vienna, Austria, Email: andreas.hueppe@tuwien.ac.at*

Introduction

One key challenge in the numerical simulation of aeroacoustic fields is the huge disparity of scales between flow structures and audible acoustic wavelengths. A volume discretization, resolving both scales from the generating vortex to the desired microphone position, not only leads to a very high number of cells but also to a very small time step size in order to minimize dissipation of the acoustic waves. Hybrid schemes in computational aeroacoustics (CAA) separate the flow from the acoustic computation by using aeroacoustic analogies. It seems adequate to use different computational grids for computing each field in an optimal manner. As a result, a factor of 100 between the cell edge lengths of flow and acoustic grids is not uncommon in low Mach number flows. The fundamental requirement is an accurate data transfer from one grid to the other with minimal interpolation errors. To cope with this task, different strategies can be applied, starting from low complexity nearest neighbour interpolation to complex volume intersections between flow and acoustic grid. Within our contribution we will investigate two approaches. The first one is a conservative interpolation strategy which features a low computational complexity but can lead to errors if certain conditions for CFD and acoustic grids do not meet certain conditions. The second scheme can be seen as an extension an copes with situations in which the flow grid has a cell size in the same range or bigger than the acoustic grid. Both schemes are investigated for two different aeroacoustic analogies.

Acoustic Analogies

The fundamental requirement for a hybrid aeroacoustic scheme is a valid aeroacoustic analogy for the given setup. The most famous one is Lighill's analogy which can be written for incompressible flows as

$$\frac{1}{c^2}\frac{\partial^2 p'}{\partial t^2} - \Delta p' = -\Delta p_{ic}. \tag{1}$$

Here, we denote the perturbation pressure by p' and the speed of sound by c. It has to be noted, that p' can only be taken as an acoustic pressure p_a in regions where $\Delta p_{ic} = 0$. In contrast to this, in low Mach number applications it is possible to split p' additively into its incompressible and compressible components (see e.g. [2]) as $p' = p_{ic} + p_a$ and apply this ansatz to (1), which yields

$$\frac{1}{c^2}\frac{\partial^2 p_a}{\partial t^2} - \Delta p_a = -\frac{1}{c^2}\frac{\partial^2 p_{ic}}{\partial t^2}. \tag{2}$$

Here, we can obtain directly the acoustic pressure p_a by taking the second time derivative of the incompressible flow pressure p_{ic}. Also other formulations including mean flow effects are possible and utilized for different applications (see e.g. [4, 3] and references therein). In most cases, taking a time or spatial derivative of the incompressible flow pressure p_{ic} remains the same in many analogies suited for incompressible flows. Obviously, the spatial properties of the source term field for the wave equation is of great importance for a grid interpolation algorithm. If the aeroacoustic wave propagation is computed using a finite element scheme, the conservative interpolation given in [1] can be utilized. Taking the variational form of the inhomogeneous wave equation as

$$\int_\Omega \varphi\, \frac{1}{c^2}\frac{\partial^2 p}{\partial t^2}\, d\Omega + \int_\Omega \nabla\varphi \cdot \nabla p\, d\Omega = \int_\Omega \varphi\, Q\, d\Omega. \tag{3}$$

in which φ denotes a test function and Q can be replaced by one of the proposed source terms in (1) or (2). Analyzing the right hand side integrals in (3), the conservative interpolation procedure is based on the assumption, that the right hand side has to be equal on the flow and acoustic grid. Thereby it is possible to write the domain integral over Ω as the sum over element integrals as

$$\int_\Omega \varphi\, Q\, d\Omega = \sum_{i=1}^{N_{CFD}} \int_{\Omega_i} \varphi\, Q\, d\Omega = \sum_{i=1}^{N_{CAA}} \int_{\Omega_i} \varphi\, Q\, d\Omega. \tag{4}$$

On this assumption, we can formulate the following algorithm

1. Compute element integrals on CFD grid according to the finite element method.

2. Search for each node in the CFD grid the containing element in the acoustic grid.

3. Compute weighted sum of all CFD nodes according to containing acoustic element.

By this procedure, we can store interpolation weights in a sparse matrix which is simply multiplied with the CFD solution vector in each time step to obtain the updated right hand side. As a result, the most time consuming part during the update of the right hand side is reading the new solution vector from the CFD.

With this algorithm, different discretization for both fields as shown e.g. in Fig. 1 can successfully be handled. In fact, this procedure can be seen as an integration of the source term field on each acoustic element. Thereby, it becomes also apparent, that it is required that at least one CFD node is contained in each acoustic element. If
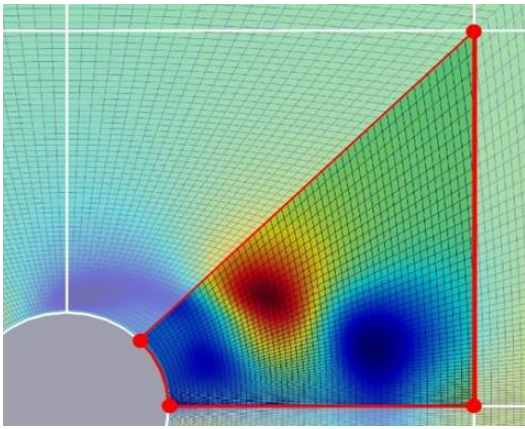
Figure 1: Typical situation of different discretization for aeroacoustics. CFD grid (blue), acoustic element (red) and contours of the source term field.

this is not the case, the interpolation error is increased significantly as we will show later.

One Dimensional Channel

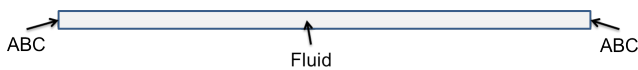For our first investigation we choose a (pseudo) one dimensional setup as depicted in Fig. 2. On both ends of

Figure 2: Thin channel setup with absorbing boundary conditions.

the channel we apply absorbing boundary conditions to avoid reflections. To excite the domain an exponential source distribution is chosen which is modulated with a sine function of given frequency

$$p_{ic} = e^{-D_1 x^2} \sin(\omega_1 t) + \frac{1}{10} e^{-D_2(x_0-x)^2} \sin(\omega_2 t) , \quad (5)$$

For the computations we choose $\omega_2 = 2\omega_1$ and $D_2 = 2D_1$ and set the origin $x = 0$ to the center of the channel. Due to the homogeneous Neumann boundary condition on the top and bottom of the channel, only plain waves can propagate. Furthermore, for the reference computations, we choose a very fine discretization $h = h_{ref}$ and monitor the acoustic signals at the end of the channel.

According to the investigated aeroacoustic formulations we need to evaluate the Laplacian or the second time derivative of the incompressible flow pressure p_{ic}. The second time derivative source field shows the expected exponential distribution as indicated in Fig. 3. The source field based on the Laplacian, on the other hand, shows a more complex distribution as shown in Fig. 4. It has to be mentioned, that this situation might even become more significant when computing in two or three space dimensions.

We investigate different levels of coarsening in the range of $h = [10 h_{ref} \dots 800 h_{ref}]$. For the coarsest discretization, the generated acoustic waves are still resolved by ten elements per smallest wavelength. By comparing the
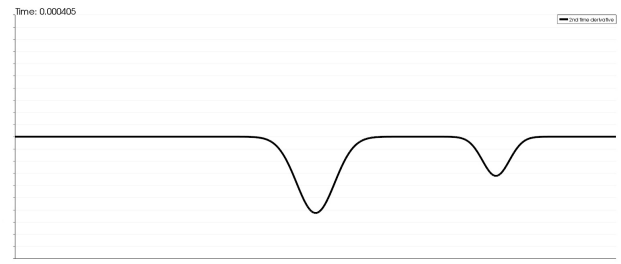

Figure 3: Instantaneous source field distribution inside the channel for $Q(x) = -\frac{\partial^2 p_{ic}}{\partial t^2}$.
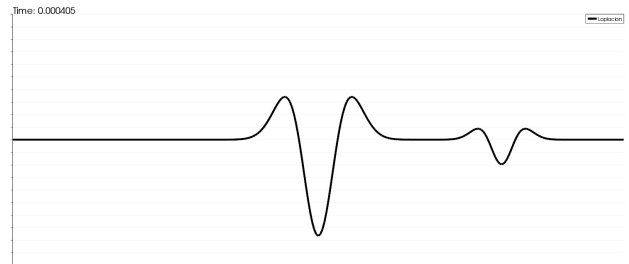

Figure 4: Instantaneous source field distribution inside the channel for $Q(x) = -\Delta p_{ic}(x)$.

monitored acoustic signals and comparing them to the reference solution we can deduce the quality of interpolation for this one dimensional example.

When using the 2nd time derivative of the flow pressure (see (2)), the simpler spatial field distribution allows a high level of grid coarsening inside the domain as visible in Fig. 5. All investigated mesh sizes allow the acoustic
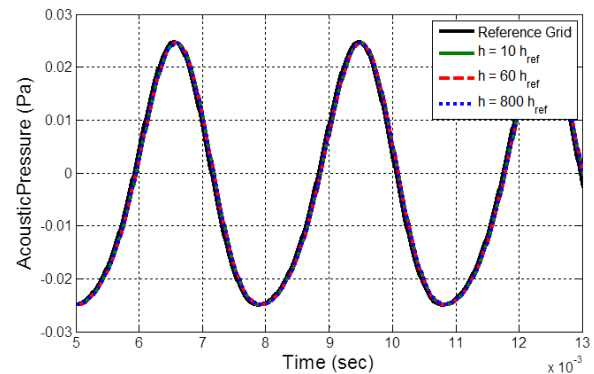

Figure 5: Results for time derivative.

signal to be transported with only minor differences to the reference signal.

The situation becomes more complicated when turning to the 2nd spatial derivative of the incompressible flow pressure (see (1)). As indicated in Fig. 6, the acoustic wave is no longer captured correctly for $h > 400 h_{ref}$. Although this seems like a high level of coarsening, we have to note, that the situation will become more complicated in case of real flow data. Especially if the computations of spatial and time derivative show numerical errors, the source term fields can get very noisy and diffracted.
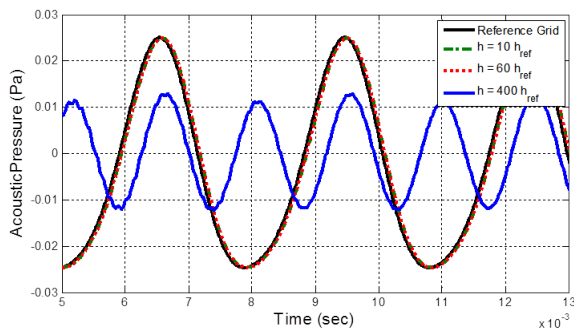
Figure 6: Results for spatial derivative.

From the one dimensional example, we can conclude that the interpolation procedure is very well suited for both formulations of acoustic source terms although the requirements on the acoustic grid are higher in the case of spatial derivatives.

Coarsening the CFD Grid

In the preceding section, we always assume that $h_{\mathrm{CFD}} << h_{\mathrm{CAA}}$. Although this assumption is, in most cases, very well fulfilled inside the source region it may be violated closer to the outflow boundary where the CFD grid is chosen very coarse in many cases and aeroacoustic sources are assumed to be of minor significance, close or equal to zero. Thereby, the interpolation error may also be of minor significance.

When computing with time derivative based source terms another effect may become important in this context. As the fluid pressure can only be determined up to a constant, when solving the incompressible Navier Stokes equations, its time derivative may lead to unphysical source term distributions. Although this effect is, in most cases, small in comparison to the significant sources, numerical errors in the CFD solution may lead to an amplification and thereby to an unphysical wave propagation. This situation is depicted in Fig. 7, showing the interpolation result of the second time derivative of the incompressible flow pressure p_{ic} as source term for a rotating setup in which two small cylinders rotate around a common axis in the center of the domain. Clearly visible are interpolation artifacts near the outflow boundary, which falsify the propagation computation.

In those cases we propose a sightly more complicated interpolation procedure, based on computing intersections of volume cells which is (with modifications) also used for data transfer between different CFD grids in finite volume codes such as OpenFOAM. The basic procedure is depicted in Fig. 8 and works on the assumption that the aeroacoustic source term is constant over the fluid cell. After we determine two cells as intersections candidates we compute the center and the volume of the intersection polyhedron. With this information it is possible to add the source contribution weighted with the intersection volume to the nodes of the acoustic element using the acoustic elements FE shape functions evaluated at
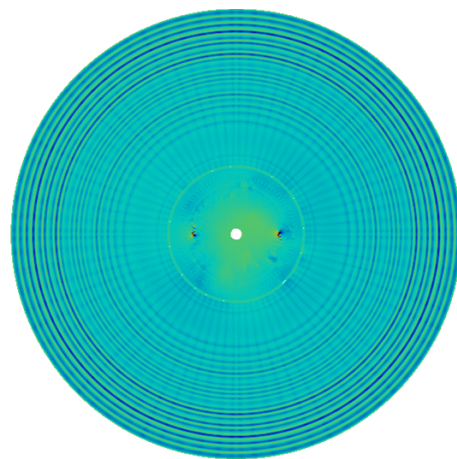

Figure 7: Artifacts due to interpolation in regions where $h_{\mathrm{CFD}} \geq h_{\mathrm{CAA}}$.
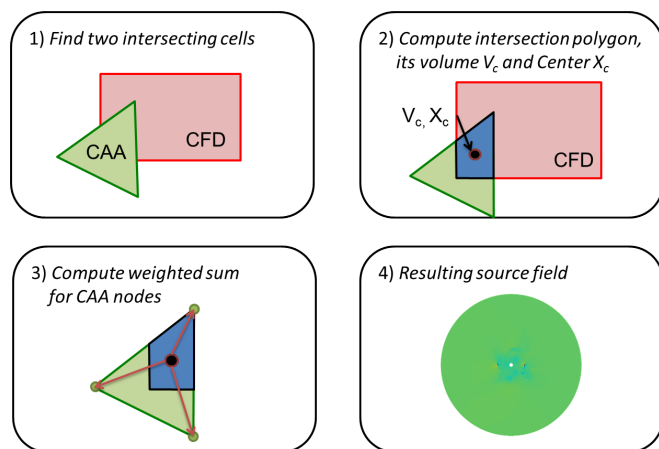

Figure 8: Steps for interpolation based on cut-volume-cell approach.

the center of the polyhedron, $Sh(\mathbf{X_c})$. For an acoustic node i this reads as

$$S_i = S_i + \mathrm{V_c} Sh_i(\mathbf{X_c}) Q(\mathbf{X_c}) \ . \tag{6}$$

Thereby we can also cover cases in which one or multiple acoustic elements are embedded into a single CFD cell. By utilizing this approach, the source term field depicted in Fig. 9 could be obtained. The color scaling corresponds to the one in Fig. 7 and we observe a smooth source term distribution indicating the reduction of the interpolation error. It is worth noting that this algorithm can be implemented with a high level of parallelism which allows to intersect also large computational grids in three space dimensions. First computations for a 32 million cell CFD grid and a 1.5 million element CAA grid resulted in a total number of 430 million cell intersection operations. Using a shared memory parallel implementation all interpolation weights were computed in 2.5 hours on a workstation with 12 threads. The standard interpolation procedure in this case took only about 15 minutes.
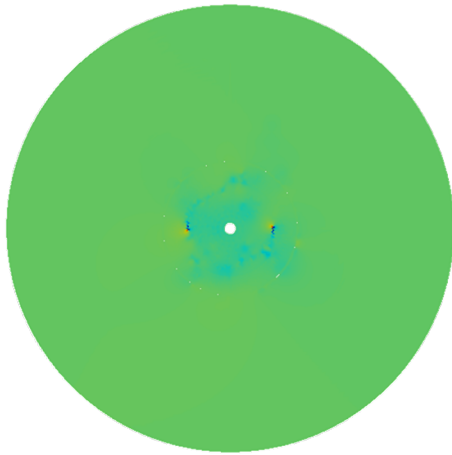
Figure 9: Source term field based on cut-volume-cell approach.

Conclusion

Within our contribution we could underline the capabilities of coarsening the acoustic grid in comparison to the flow grid. The approach utilized so far, allows the acoustic grid to be defined much coarser than the CFD grid as long as all relevant acoustic waves are captured. Also we could show that the utilization of the 2nd spatial derivative of the flow pressure p_{ic} as source term require much finer acoustic grids due to a more complex source field distribution. As a rule of thumb, the one dimensional computations indicate that the smallest relevant vortex needs to be resolved with two acoustic cells whereas the 2nd time derivative of the flow pressure as source term allows at least a two times coarser grid. Finally, we could demonstrate how it is possible to avoid interpolation artifacts by utilizing a cut-cell-volume approach in regions where the CFD mesh is coarser than the acoustic grid. Furthermore, a combination of both approaches is feasible and might help to decrease the overall computational effort.

References

[1] Kaltenbacher M., Escobar M., Becker S., Ali I.: Numerical simulation of flow-induced noise using LES/SAS and Lighthill's acoustic analogy. International Journal for Numerical Methods in Fluids, 2010

[2] Ewert A., Schröder W.: Acoustic perturbation equations based on flow decomposition via source filtering. Journal of Computational Physics 188 (2003), 365-398

[3] Hüppe A. and Kaltenbacher M.: Spectral finite elements for computational aeroacoustics using acoustic perturbation equations. Journal of Computational Acoustics, 2012

[4] Hüppe A., Grabinger J., Kaltenbacher M., Reppenhagen A., Dutzler G., Kühnel. W.: A Non-Conforming Finite Element Method for Computational Aeroacoustics in Rotating Systems. In Proceedings of the 20th AIAA/CEAS Aeroacoustics Conference, AIAA-2014, 2014. 16-20 June 2014, Atlanta, USA. CD-ROM Proceedings